AIP | The Journal of Chemical Physics
FREE ACCESS THROUGH 2013

A hybrid kinetic Monte Carlo method for simulating silicon films grown by plasma-enhanced chemical vapor deposition

D. G. Tsalikis, C. Baig, V. G. Mavrantzas, E. Amanatides, and D. Mataras

Citation: The Journal of Chemical Physics **139**, 204706 (2013); doi: 10.1063/1.4830425
View online: http://dx.doi.org/10.1063/1.4830425
View Table of Contents: http://scitation.aip.org/content/aip/journal/jcp/139/20?ver=pdfcov
Published by the AIP Publishing

Re-register for Table of Content Alerts

Create a profile.
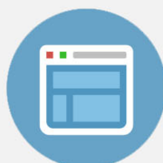
Sign up today!

This article is copyrighted as indicated in the article. Reuse of AIP content is subject to the terms at: http://scitation.aip.org/termsconditions. Downloaded to IP: 114.70.7.203 On: Tue, 10 Dec 2013 00:58:03

A hybrid kinetic Monte Carlo method for simulating silicon films grown by plasma-enhanced chemical vapor deposition

D. G. Tsalikis,[1] C. Baig,[2] V. G. Mavrantzas,[1,a)] E. Amanatides,[1] and D. Mataras[1,a)]
[1]*Department of Chemical Engineering, University of Patras, Patras GR26500, Greece*
[2]*School of Nano-Bioscience and Chemical Engineering, Ulsan National Institute of Science and Technology (UNIST), Ulsan 689-798, South Korea*

(Received 31 July 2013; accepted 31 October 2013; published online 26 November 2013)

We present a powerful kinetic Monte Carlo (KMC) algorithm that allows one to simulate the growth of nanocrystalline silicon by plasma enhanced chemical vapor deposition (PECVD) for film thicknesses as large as several hundreds of monolayers. Our method combines a standard *n*-fold KMC algorithm with an efficient Markovian random walk scheme accounting for the surface diffusive processes of the species involved in PECVD. These processes are extremely fast compared to chemical reactions, thus in a brute application of the KMC method more than 99% of the computational time is spent in monitoring them. Our method decouples the treatment of these events from the rest of the reactions in a systematic way, thereby dramatically increasing the efficiency of the corresponding KMC algorithm. It is also making use of a very rich kinetic model which includes 5 species (H, SiH_3, SiH_2, SiH, and Si_2H_5) that participate in 29 reactions. We have applied the new method in simulations of silicon growth under several conditions (in particular, silane fraction in the gas mixture), including those usually realized in actual PECVD technologies. This has allowed us to directly compare against available experimental data for the growth rate, the mesoscale morphology, and the chemical composition of the deposited film as a function of dilution ratio. © *2013 AIP Publishing LLC*. [http://dx.doi.org/10.1063/1.4830425]

I. INTRODUCTION

Plasma enhanced chemical vapor deposition (PECVD) is a very popular and widely used technique for growing thin films of silicon (Si) for many practical applications in electronics,[1] optoelectronics,[2] and photovoltaics.[3,4] The method employs silane and hydrogen as the source gas which is decomposed by collision with energetic electrons (that are generated in a gas discharge). It is a very complex silane-hydrogen-based process involving several gas-phase reactions in a chamber as well as surface reactions at the substrate with species transporting in the chamber. By exploiting the presence of reactive radicals, rather high growth rates (>1 nm/s) can be obtained; this renders the technique of industrial interest[5,6] allowing for the fast deposition of thin films even at low or moderately low temperatures. By tuning the growth parameters, PECVD can be used to grow epitaxial, amorphous, and microcrystalline (μc) or nanocrystalline (nc) films. μc-Si and nc-Si films, in particular, are attracting wide interest nowadays as promising absorber layers for the production of solar cells with a good efficiency/cost ratio.[4]

From a theoretical or modeling point of view, our understanding of PECVD is still quite limited,[6,7] and this is due to several reasons: (a) The presence of plasma introduces a non-trivial degree of complexity, mainly in terms of the many different species created and subsequently impinging the film. (b) Identifying all chemical species involved and all physico-chemical processes taking place (especially the surface-plasma interactions) is a formidable task. (c) Obtaining accurate rate constants for the chemical processes involved is also challenging. (d) Even if these processes and their kinetics were all known, simulating the full process would require a tremendous effort because of the many different time and length scales involved. As a result, one is in the need first to resort to different methods to tackle specific problems in a given window of time and length scales, and second to integrate results from these different methods to develop hierarchical approaches or multi-level simulation schemes.

In the literature, several models have been proposed in an effort to simulate and elucidate the molecular mechanisms that govern the growth of plasma deposited silicon. Continuum models (which are applicable when the characteristic length is significantly greater than the molecular scale) have been invoked in order to study the evolution of grain microstructure, surface roughness, and texture during polycrystalline film growth[8,9] based on a set of partial differential equations describing the motion of grain boundaries. However, they are typically characterized by limited predictive capability because they often fail to account for the effects of important microscopic defects such as vacancies and voids[10,11] that are normally formed during film growth. In addition, it is not straightforward how to incorporate nucleation of new grains, a process that occurs during nanostructured film growth.[12] Discrete models, on the other hand, have been shown to be capable of capturing such microscopic processes as diffusion, grain boundary migration,[13] vacancy entrapment, and void formation.[14,15] For instance, Smith *et al.*[15] explored the dynamical mechanisms of void formation and interactions between voids and grain

a)Authors to whom correspondence should be addressed. Electronic addresses: vlasis@chemeng.upatras.gr and dim@plasmatech.gr.

 © 2013 AIP Publishing LLC

This article is copyrighted as indicated in the article. Reuse of AIP content is subject to the terms at: http://scitation.aip.org/termsconditions. Downloaded to IP: 114.70.7.203 On: Tue, 10 Dec 2013 00:58:03

boundaries during film growth in bicrystals. By adopting a rigid lattice neglecting details of atomic vibrations, a much less computationally expensive discrete model such as the kinetic Monte Carlo (KMC) method[16,17] can be applied. KMC has thus been employed with great success to study several problems involving surface reaction kinetics.[18–22] Wetterauer[21] and co-workers employed a one-dimensional KMC model to simulate CVD amorphous silicon growth; predictions for the growth rate and hydrogen content were found to be in good quantitative agreement with experimental data. KMC-based methodologies using simplified chemical models have also been proposed capable of achieving films amounting to 10^4 monolayers in thickness.[23–27] Novicov *et al.*[28] developed an efficient KMC algorithm, which is capable of growing films up to some hundreds of monolayers by introducing an environment-dependent crystallization probability and showed a reasonable prediction for the film growth rate and degree of crystallinity occurring in nanocrystalline films under a low-energy PECVD. In their chemical model,[29–31] however, important dynamical mechanisms such as surface diffusion and formation of defects were neglected. On the other hand, Pandey *et al.*[32] conducted more detailed KMC simulations by incorporating various surface growth reactions,[6,33–39] including diffusion events of surface radicals. Their results (e.g., for the concentration of surface silicon hydride) appeared to be in qualitatively good agreement with available experimental data over a broad range of temperatures ($T = 325-650$ K); however, the film thicknesses addressed in their work were limited to those corresponding to a rather small number of monolayers.

Various KMC models have been proposed to study how the growth interface roughens during film deposition in a single crystal[23–27,40–44] or to simulate film growth of polycrystalline films. One approach is to use multiple lattices to account for different grain orientations. However, this approach is computationally quite expensive, thus capable of simulating film growth only for short time scales.[45–48] For example, Bruschi *et al.*[45] utilized a quasi-continuous coordinate system in which the simulated film was represented by a two-dimensional array of square cells with exact atomic positions within each cell. Although this method allows for different grain orientations, the simulated films were at most one monolayer thick. Based on a similar approach, Rubio *et al.*[47] were able to grow comparatively larger films, but still less than 50 monolayers in thickness. Huang and Zhou[46] proposed an improved method called memory-efficient algorithm to map multiple lattices onto a single lattice; still, however, only films less than 100 monolayers thick could be simulated. Another useful approach to simulate the growth of polycrystalline films is to incorporate some features of the Q-state Potts model originally proposed by Srolovitz and co-workers.[49,50] However, such an approach does not quantitatively account for void formation; in addition, only deposition times spanning less than 100 monolayers can be tracked.[20,51–56] Ruan and Schun[57] have recently proposed an efficient KMC method which includes diffusion processes and allows for the formation of voids and vacancies during film growth. The method is capable of simulating nanocrystalline film with kinetic roughening, vacancy entrapment, grain nucleation and grain evolution. Despite that their method could access a film thickness that can accommodate many nanoscale grains, it has been applied so far only to a two-dimensional lattice system in order to reduce the computational cost.

Clearly, we are in the need of developing more efficient (i.e., capable of addressing several hundreds of monolayers) but also more accurate three-dimensional KMC models based on a comprehensive set of surface reactions without losing important physical mechanisms such as diffusion. And this is the main contribution of the present study. We propose a powerful KMC model that allows one to study the structural and kinetic properties of film growth under technologically relevant conditions of pressure P (=4 mbar), power (= 310 mW/cm^2), total flow rate (=1 slm (standard litres per minute)), and silane mole fraction in gas phase or silane dilution ratio (DR) (1%–6%) in a medium scale plasma reactor. Based on a carefully chosen set of reactive species (radicals), a comprehensive set of surface reactions, and an efficient implementation of the diffusion processes, our KMC algorithm offers a quantitative treatment of the most important physical and chemical mechanisms involved during the growth of sufficiently thick nanoscale Si films within reasonable computational time. Input data for the fluxes of radicals are provided from a well-tuned plasma fluid model.[58,59] The three-dimensional KMC method developed in this work is able to follow rather accurately the growth of Si films for thicknesses up to several tens of nanometers with moderate computational resources. This has allowed us to carry out simulations for various DRs and thus to compare quantitatively with available experimental data for results such as film growth rate and hydrogen content under similar conditions.

The present work is part of a more systematic project aiming at predicting structure and morphology in films grown by PECVD as a function of the growth parameters. Our main objective is to develop a hierarchical modeling approach that will allow us to: (a) tackle the problem of local crystallization depending on processing conditions, (b) elucidate the microscopic mechanisms behind the growth of epitaxial, amorphous, and micro- or nanocrystalline films, and (c) suggest optimal growth parameters that could help realize further improvements of the PECVD process. To this, we propose a three-step approach as follows:

(a) First, a reliable but phenomenological kinetic model is employed on the basis of a coarse-grained description for the important species involved in the process to study film deposition and growth across several length and time scales; the method to use here is KMC on a lattice geometry and the target is to get films with realistic structural (density and voids) and surface (texture and roughness) properties as a function of the operating conditions (silane dilution ratio and fluxes). This will give us the first insight into the overall structure of the deposited films.
(b) In the second stage of our work, the coarse-grained KMC model will be mapped onto an atomistic model through reverse mapping: the important species considered in stage (a) will be mapped here to silicon and hydrogen

This article is copyrighted as indicated in the article. Reuse of AIP content is subject to the terms at: http://scitation.aip.org/termsconditions. Downloaded to IP: 114.70.7.203 On: Tue, 10 Dec 2013 00:58:03

atoms, and the method to use is atomistic Monte Carlo. Through the design of an efficient set of Monte Carlo moves, the help of accurate atomistic models,[60,61] and the Metropolis criterion for accepting new (i.e., trial) configurations from an old state, we will be able to fully optimize the structural properties and nanoscale morphology of the silicon films obtained in stage (a). Our target here is to simulate in detail the semi-crystalline nature of the system at the atomic level (i.e., to quantify the presence of crystalline, amorphous and interfacial zones in the deposited films). This is not possible with the KMC algorithm for two reasons: the first is that it is realized on a fully occupied lattice geometry; the second is that it involves coarse-grained units (the chemical species considered in the underlying kinetic model) which prevents characterizing the film structure around any site at scales that extend beyond the length scale of the nearest neighbors. Step (b) is still underway; but when it is completed it will result in a powerful MC code that, given an initial film configuration from step (a), will be able to optimize its structure by driving the system to the state of the correct thermodynamic equilibrium for the given set of temperature and pressure conditions.[62]

(c) The third and final step of our work will be to run the two codes (the KMC code developed in stage (a) and the Metropolis Monte Carlo code developed in stage (b)) together in a hierarchical way in order to be able to monitor and simulate the growth process of thin silicon films deposited during PECVD at all length scales. Here, the KMC code will be executed first for a certain period of time (e.g., a few microseconds) to get an initial condition for the film and then the atomistic Monte Carlo code will be turned on to optimize the structure of this film. The optimized structure from the atomistic MC algorithm will be fed back to the KMC model and this will be run again for another period of time. And all this will be continued until time scales are reached comparable to those realized in the corresponding industrial process.

This paper is concerned with step (a) of the approach and is organized as follows: We begin in Sec. II with a detailed presentation of the kinetic events (the chemical model) accounted for in our algorithm and their rates. The new KMC algorithm is described in Sec. III. Numerical results are presented and discussed in Sec. IV, and conclusions are given in Sec. V.

II. CHEMICAL MODEL

The rate processes accounted for in our KMC algorithm are reported in Table I. The corresponding chemical model includes five important chemically reactive gas-phase species: hydrogen (H), monohydride (SiH), dihydride (SiH_2), trihydride (SiH_3), and disilyl (Si_2H_5) radicals. These are the main (electrically neutral) species that are considered to participate in film growth under industrially relevant dust-free or low dust plasma conditions. The gas-phase species with relatively low reactivity (SiH_3, Si_2H_5, and H radicals) exhibit similar reaction pathways. They can be either directly chemisorbed onto dangling bond (DB) sites leading to film growth (R1−R3) or physisorbed on hydrogen passivated (H-pass) sites (R7−R9). From the physisorbed states, they can undergo a variety of physico-chemical reaction processes such as surface diffusion (R10−R12), desorption (R27−R29), formation of stable gas-phase molecules (R16−R21) via a Langmuir-Hinshelwood (LH) mechanism, diffusive chemisorption onto a neighboring DB site involving film growth (R13, R15), hydrogen passivation of a DB site (R14), and abstraction of surface hydrogen by physisorbed radicals (R22−R24) leaving behind a dangling bond. We note here that the Eley-Rideal (ER) mechanism (e.g., a direct abstraction of surface hydrogen by a gas-phase radical), as implemented in our KMC model, involves two separate reaction steps: (i) physisorption of gas-phase radicals on the surface (R7−R9) and (ii) subsequent abstraction of the surface atoms (R22−R24). On the other hand, highly reactive species such as SiH_2 and SiH are taken to be directly chemisorbed onto either DB or H-pass sites (R4−R6). Bulkilization reactions between dangling bond sites (R25) and H-pass sites (R26) are also included in our KMC model. All radicals from the gas phase are assumed to impinge upon the surface vertically (at right angle), implying that no shadowing effects are accounted for in our scheme. This rich chemical model allows us to investigate the role of important microscopic molecular mechanisms underlying film growth under practically relevant conditions and how they affect the nano-structure of the resulting film as a function of deposition conditions.

We mention here that, in the initial stage of our model development, the applied chemical scheme bears many similarities with the surface diffusion model proposed by Matsuda,[63–65] where surface species diffusivity plays a very important role. As the main target is to simulate μc-Si:H thin film growth from highly diluted SiH_4 in H_2 discharges, during the growth, the substrate should be expected to be exposed to large fluxes of the highly mobile hydrogen atoms.[66] The high hydrogen flux combined with ion bombardment (not included in our model) can alter the mobility and energetics of surface species such as H, SiH_3, and Si_2H_5. There are also quite strong experimental indications (Step Coverage method, Quadruple Threshold Ionization Mass spectrometry, *in situ* Fourier-transform Infrared Spectrometer) of the species surface diffusion enhancement in μc-Si:H deposition.[67–69] These are mainly based on the significant increase of SiH_3 surface loss probability without a change in the sticking coefficient when we compare deposition conditions of μc-Si:H to a-Si:H thin films. On the other hand, there are findings based on *ab initio* calculations[29,30] that predict a limited diffusivity of silicon hydrides on fully hydrogenated surfaces. Thus, investigation of the effect of the diffusivity of all species included in our model (H, SiH_3, and Si_2H_5) on its predictions referring to film growth rate and H-content should be the next step.

III. METHODOLOGY

A. Reaction rate evaluation

The reaction mechanisms underlying silicon film growth that are considered in our work include athermal (i.e., no activation energy barrier or simply barrierless) and thermally

This article is copyrighted as indicated in the article. Reuse of AIP content is subject to the terms at: http://scitation.aip.org/termsconditions. Downloaded to IP: 114.70.7.203 On: Tue, 10 Dec 2013 00:58:03

TABLE I. Surface kinetic events incorporated in the present kinetic Monte Carlo algorithm for simulating the process of plasma enhanced chemical vapor deposition of silicon thin films with gas-phase species (H, SiH_3, SiH_2, SiH, and Si_2H_5). The subscript "(g)" denotes gas-phase species and the subscripts "(s)" and "(s′)", respectively, the chemisorbed and physisorbed surface species. As a Si atom can form four bonds, the surface sites Si_{4-x}-Si-H_x and Si_{3-x}-Si-H_x (or Si_{4-x}-Si-H_{x-1}) indicate hydrogen passivated (fully coordinated) and dangling bond sites, respectively. The main chemical species directly involved in the physicochemical reactions are colored for clarity.

Reaction Type	Description[a]	Reaction Mechanism	Index Information
R1	SiH_3(g) Chemisorptions on DB	$\mathbf{SiH_3(g)} + Si_{3-x}Si\text{-}H_x \rightarrow Si_{3-x}\text{-}Si\text{-}H_x\mathbf{SiH_3(s)}$	x={0, 1, 2}
R2	H(g) Chemisorptions on DB	$\mathbf{H(g)} + Si_{3-x}Si\text{-}H_x \rightarrow Si_{3-x}\text{-}Si\text{-}H_x\mathbf{H(s)}$	x={0, 1, 2}
R3	Si_2H_5(g) Chemisorptions on DB	$\mathbf{Si_2H_5(g)} + Si_{3-x}\text{-}Si\text{-}H_x \rightarrow Si_{3-x}\text{-}Si\text{-}H_x\mathbf{Si_2H_5(s)}$	x={0, 1, 2}
R4	SiH_2(g) Chemisorptions on DB	$\mathbf{SiH_2(g)} + Si_{3-x}\text{-}Si\text{-}H_x \rightarrow Si_{3-x}\text{-}Si\text{-}H_x\mathbf{SiH_2(s)}$	x={0, 1, 2}
R5	SiH_2(g) chemisorption on H-pass	$\mathbf{SiH_2(g)} + Si_{4-x}\text{-}Si\text{-}\mathbf{H_x} \rightarrow Si_{4-x}\text{-}Si\text{-}\mathbf{H_{x-1}SiH_3(s)}$	x={1, 2, 3}
R6	SiH(g) chemisorption on H-pass	$\mathbf{SiH(g)} + Si_{4-x}\text{-}Si\text{-}\mathbf{H_x} \rightarrow Si_{4-x}\text{-}Si\text{-}\mathbf{H_{x-1}SiH_2(s)}$	x={1, 2, 3}
R7	SiH_3(g) physisorption	$\mathbf{SiH_3(g)} + Si_{4-x}\text{-}Si\text{-}H_x \rightarrow Si_{4-x}\text{-}Si\text{-}H_x\mathbf{SiH_3(s')}$	x={1, 2, 3}
R8	H(g) physisorption	$\mathbf{H(g)} + Si_{4-x}\text{-}Si\text{-}H_x \rightarrow Si_{4-x}\text{-}Si\text{-}H_x\mathbf{H(s')}$	x={1, 2, 3}
R9	Si_2H_5(g) physisorption	$\mathbf{Si_2H_5(g)} + Si_{4-x}\text{-}Si\text{-}H_x \rightarrow Si_{4-x}\text{-}Si\text{-}H_x\mathbf{Si_2H_5(s')}$	x={1, 2, 3}
R10	SiH_3(s′) diffusion	$Si_{4-x}\text{-}Si\text{-}H_x\mathbf{SiH_3(s')} + Si_{4-y}\text{-}Si\text{-}H_y \rightarrow Si_{4-x}\text{-}Si\text{-}H_x + Si_{4-y}\text{-}Si\text{-}H_y\mathbf{SiH_3(s')}$	x, y={1, 2, 3}
R11	H(s′) diffusion	$Si_{4-x}\text{-}Si\text{-}H_x\mathbf{H(s')} + Si_{4-y}\text{-}Si\text{-}H_y \rightarrow Si_{4-x}\text{-}Si\text{-}H_x + Si_{4-y}\text{-}Si\text{-}H_y\mathbf{H(s')}$	x, y={1, 2, 3}
R12	Si_2H_5(s′) diffusion	$Si_{4-x}\text{-}Si\text{-}H_x\mathbf{Si_2H_5(s')} + Si_{4-y}\text{-}Si\text{-}H_y \rightarrow Si_{4-x}\text{-}Si\text{-}H_x + Si_{4-y}\text{-}Si\text{-}H_y\mathbf{Si_2H_5(s')}$	x, y={1, 2, 3}
R13	SiH_3(s′) diffusive chemisorption on neighboring DB	$Si_{4-x}\text{-}Si\text{-}H_x\mathbf{SiH_3(s')} + Si_{3-y}\text{-}Si\text{-}H_y \rightarrow Si_{4-x}Si\text{-}H_x + Si_{3-y}\text{-}Si\text{-}H_y\mathbf{SiH_3(s)}$	x={1, 2, 3}, y={0, 1, 2}
R14	H(s′) diffusive chemisorption on neighboring DB	$Si_{4-x}\text{-}Si\text{-}H_x\mathbf{H(s')} + Si_{3-y}\text{-}Si\text{-}H_y \rightarrow Si_{4-x}Si\text{-}H_x + Si_{3-y}\text{-}Si\text{-}H_y\mathbf{H(s)}$	x={1, 2, 3}, y={0, 1, 2}
R15	Si_2H_5(s′) diffusive chemisorption on neighboring DB	$Si_{4-x}\text{-}Si\text{-}H_x\mathbf{Si_2H_5(s')} + Si_{3-y}\text{-}Si\text{-}H_y \rightarrow Si_{4-x}\text{-}Si\text{-}H_x + Si_{3-y}\text{-}Si\text{-}H_y\mathbf{Si_2H_5(s)}$	x={1, 2, 3}, y={0, 1, 2}
R16	LH disilane abstraction	$Si_{4-x}\text{-}Si\text{-}H_x\mathbf{SiH_3(s')} + Si_{4-y}\text{-}Si\text{-}H_y\mathbf{SiH_3(s')} \rightarrow Si_{4-x}\text{-}Si\text{-}H_x + Si_{4-y}\text{-}Si\text{-}H_y + \mathbf{Si_2H_6(g)}$	x, y={1, 2, 3}
R17	LH silane formation	$Si_{4-x}\text{-}Si\text{-}H_x\mathbf{H(s')} + Si_{4-y}\text{-}Si\text{-}H_y\mathbf{SiH_3(s')} \rightarrow Si_{4-x}\text{-}Si\text{-}H_x + Si_{4-y}\text{-}Si\text{-}H_y + \mathbf{SiH_4(g)}$	x, y={1, 2, 3}
R18	LH trisilane formation	$Si_{4-x}\text{-}Si\text{-}H_x\mathbf{SiH_3(s')} + Si_{4-y}Si\text{-}H_y\mathbf{Si_2H_5(s')} \rightarrow Si_{4-x}\text{-}Si\text{-}H_x + Si_{4-y}Si\text{-}H_y + \mathbf{Si_3H_8(g)}$	x, y={1, 2, 3}
R19	LH H_2 formation	$Si_{4-x}\text{-}Si\text{-}H_x\mathbf{H(s')} + Si_{4-y}\text{-}Si\text{-}H_y\mathbf{H(s')} \rightarrow Si_{4-x}\text{-}Si\text{-}H_x + Si_{4-y}Si\text{-}H_y + \mathbf{H_2(g)}$	x, y={1, 2, 3}
R20	LH disilane formation	$Si_{4-x}\text{-}Si\text{-}H_x\mathbf{H(s')} + Si_{4-y}\text{-}Si\text{-}H_y\mathbf{Si_2H_5(s')} \rightarrow Si_{4-x}\text{-}Si\text{-}H_x + Si_{4-y}Si\text{-}H_y + \mathbf{Si_2H_6(g)}$	x, y={1, 2, 3}
R21	LH tetra-silane formation	$Si_{4-x}\text{-}Si\text{-}H_x\mathbf{Si_2H_5(s')} + Si_{4-y}\text{-}Si\text{-}H_y\mathbf{Si_2H_5(s')} \rightarrow Si_{4-x}\text{-}Si\text{-}H_x + Si_{4-y}\text{-}Si\text{-}H_y + \mathbf{Si_4H_{10}(g)}$	x, y={1, 2, 3}
R22	ER H abstraction by SiH_3(s′)	$Si_{4-x}\text{-}Si\text{-}\mathbf{H_xSiH_3(s')} \rightarrow Si_{4-x}\text{-}Si\text{-}\mathbf{H_{x-1}} + \mathbf{SiH_4(g)}$	x={1, 2, 3}
R23	ER H abstraction by H(s′)	$Si_{4-x}\text{-}Si\text{-}\mathbf{H_xH(s')} \rightarrow Si_{4-x}\text{-}Si\text{-}\mathbf{H_{x-1}} + \mathbf{H_2(g)}$	x={1, 2, 3}
R24	ER H abstraction by Si_2H_5(s′)	$Si_{4-x}\text{-}Si\text{-}\mathbf{H_xSi_2H_5(s')} \rightarrow Si_{4-x}\text{-}Si\text{-}\mathbf{H_{x-1}} + \mathbf{Si_2H_6(g)}$	x={1, 2, 3}
R25	Bulkilization DB sites	$Si_{3-x}-\underset{H_x}{\mathbf{Si}} + \underset{H_y}{\mathbf{Si}}-Si_{3-y} \rightarrow Si_{3-x}-\underset{H_x}{\mathbf{Si}} - \underset{H_y}{\mathbf{Si}}-Si_{3-y}$	x, y={0, 1, 2}
R26	Bulkilization H-pass sites	$Si_{4-x}-\underset{H_x}{\mathbf{Si}} + \underset{H_y}{\mathbf{Si}}-Si_{4-y} \rightarrow Si_{4-x}-\underset{H_{x-1}}{\mathbf{Si}} - \underset{H_{y-1}}{\mathbf{Si}}-Si_{4-y} + \mathbf{H_2}(g)$	x, y={1, 2, 3}
R27	SiH_3(s) desorption	$Si_{4-x}\text{-}Si\text{-}H_x\mathbf{SiH_3(s')} \rightarrow Si_{4-x}\text{-}Si\text{-}H_x + \mathbf{SiH_3(g)}$	x={1, 2, 3}
R28	H(s) desorption	$Si_{4-x}\text{-}Si\text{-}H_x\mathbf{H(s')} \rightarrow Si_{4-x}\text{-}Si\text{-}H_x + \mathbf{H(g)}$	x={1, 2, 3}
R29	Si_2H_5(s) desorption	$Si_{4-x}\text{-}Si\text{-}H_x\mathbf{Si_2H_5(s')} \rightarrow Si_{4-x}\text{-}Si\text{-}H_x + \mathbf{Si_2H_5(g)}$	x={1, 2, 3}

[a]DB and H-pass represent dangling bond and hydrogen passivated sites, respectively. LH (R16−R21) and ER (R22−R24) denote Langmuir-Hinshelwood and Eley-Rideal reaction mechanisms, respectively.

activated kinetic events. The first group encompasses all reactions (R1−R9 in Table I) involving the gas-phase species ($H_{(g)}$, $SiH_{3(g)}$, $SiH_{2(g)}$, $SiH_{(g)}$, and $Si_2H_{5(g)}$) impinging upon the film surface (i.e., chemisorption onto DB and hydrogen H-pass sites, and physisorption to H-pass sites). The second group includes all the surface reactions without gas-phase species (i.e., surface diffusion, Langmuir-Hinshelwood (LH) reactions, hydrogen abstraction, desorption, and bulkilization). Based on the fundamental kinetic theory of gases, we have evaluated the reaction rate r of each barrierless event

This article is copyrighted as indicated in the article. Reuse of AIP content is subject to the terms at: http://scitation.aip.org/termsconditions. Downloaded to IP: 114.70.7.203 On: Tue, 10 Dec 2013 00:58:03

TABLE II. Sticking coefficients for athermal reactions and reaction rates for thermally activated reactions employed in the present chemical model.

Athermal reactions		Thermally activated reactions			
Reaction type	Sticking coefficient	Reaction type	Reaction rate (s^{-1})	Reaction type	Reaction rate (s^{-1})
R1	0.6	R10	5.8×10^{9}	R19	1.14×10^{10}
R2	0.8	R11	7.94×10^{9}	R20	1.82×10^{7}
R3	0.8	R12	2.27×10^{9}	R21	1.22×10^{7}
R4	0.5	R13	7.16×10^{1}	R22	4.61×10^{3}
R5	0.6	R14	1.12×10^{3}	R23	5.82×10^{3}
R6	0.8	R15	2.27×10^{9}	R24	4.61×10^{3}
R7	0.5	R16	2.13×10^{7}	R25	4.43×10^{3}
R8	0.4	R17	5.97×10^{9}	R26	7.12×10^{-2}
R9	0.45	R18	1.64×10^{7}		

by the following equation:

$$r = J s_c N_A \sigma, \tag{1}$$

where s_c is the local sticking coefficient, N_A the Avogadro number, J the flux of gas-phase radical involved, and σ the average area per surface site. The flux J can be calculated as

$$J = \mu \langle u \rangle n, \tag{2}$$

where μ is the mole fraction of the gas-phase species, $\langle u \rangle$ the average velocity, and n the total number density. From the kinetic theory of gases, the average velocity $\langle u \rangle$ is given by

$$\langle u \rangle = \sqrt{\frac{8 k_B T}{\pi m}}, \tag{3}$$

where k_B is the Boltzmann constant, T the gas phase temperature, and m the molecular mass. Combining Eqs. (1)–(3) we obtain

$$r = \mu \sqrt{\frac{8 k_B T}{\pi m}} n s_c N_A \sigma. \tag{4}$$

On the other hand, the reaction rate of a thermally activated kinetic event can be estimated by using the standard Arrehnius-type equation:

$$r = \upsilon_0 e^{-E_a / k_B T}, \tag{5}$$

where υ_0 is the attempt frequency prefactor (s^{-1}) and E_a the activation energy barrier. The reaction rates involving the desorption of the physisorbed radicals (R27–R29) are not calculated via Eq. (5); instead, they are considered to be equal to the corresponding physisorption rates (R7–R9).

The resulting rate values for each reaction event considered in our KMC simulations[33–39,70–74] are given in Table II. In this table, for the thermally activated reactions we explicitly report the corresponding reaction rates; for the athermal ones, on the other hand, only the value of the sticking coefficients is reported (since they typically depend on gas phase composition).

B. The *n*-fold kinetic Monte Carlo method

To simulate and monitor the temporal evolution of the grown Si films, we applied a standard *n*-fold MC scheme[16,17] on a diamond lattice geometry. In order to generate the total list of all possible events at each KMC step, we introduced an efficient propagator that, for each surface site, keeps track of the coordination number of all surface Si atoms up to the next-nearest neighbors. A parallel computing procedure was implemented to efficiently generate the full list of possible events for each surface site by evenly distributing all reactive sites into multiple processes; this information is exchanged between different processes during a KMC execution.

The algorithm proceeds as follows: at each KMC step a complete list of possible reactions for all surface sites is constructed, and then a reaction event j is randomly selected according to the following equation:

$$\frac{\sum_{i=1}^{i=j-1} r_i}{R} < \xi_1 < \frac{\sum_{i=1}^{i=j} r_i}{R}, \tag{6}$$

where

$$R = \sum_{i=1}^{i=M} r_i. \tag{7}$$

Here ξ_1 is a random number generated from a uniform distribution, $\xi_1 \in (0, 1)$, M denotes the total number of possible reaction events at present step, and r_i is the reaction rate of the ith event. The corresponding time increment δt through this KMC step is calculated by

$$\delta t = -\frac{\ln(\xi_2)}{R}, \tag{8}$$

where ξ_2 is another random number drawn from a uniform distribution. In the next KMC step, the total list of possible events for each surface site is updated based on the new surface topology and the same procedure is carried out. And all this is continued for as many times as needed until the desired film thickness is reached.

C. Diffusion modelling

The reaction events incorporated into our KMC model span a very broad range of time scales, e.g., $\sim 1-10^{12}$ s. Surface diffusion reactions (R10−R12 in Table I), in particular, are seen to occur too often and be extremely fast compared to the rest of reactions, implying that the majority of computational time is spent in monitoring the diffusive motion of physisorbed radicals. To be more specific, in Fig. 1 we present the probability distribution of reaction events resulting from a conventional, brute force execution of the KMC simulation (for $T = 453$ K, $P = 4$ mbar, silane DR = 6%) up to 0.5 s. It is clear that the vast majority (≈99.996%) of computational time is taken over by the fast surface diffusion of adsorbed radicals; in contrast, only a small fraction of the computational time is spent on reactions (R1−R6, R13 and R15 in Table I) leading to film growth. Despite this, these diffusive reactions should not be neglected, because the mobility of physisorbed species plays an important role in determining the overall film structure. This has led us to devise an efficient scheme for speeding up the overall computational time while simultaneously not disregarding diffusive processes. Our method is to treat the diffusion processes separately from the remaining reactions: the fast diffusive motion of the physisorbed species is approximated as a three dimensional (3D) Markovian random walk process while all other reactions are

This article is copyrighted as indicated in the article. Reuse of AIP content is subject to the terms at: http://scitation.aip.org/termsconditions. Downloaded to IP: 114.70.7.203 On: Tue, 10 Dec 2013 00:58:03

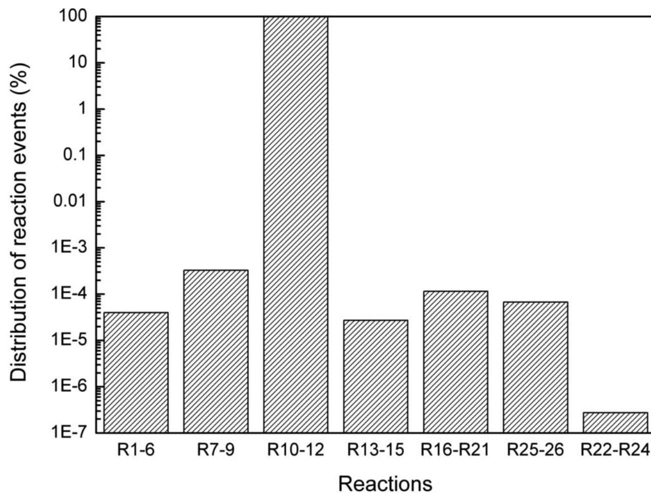

FIG. 1. Probability distribution of the occurrence of reaction events considered in the present KMC simulations during a brute force execution of the corresponding algorithm at $T = 453$ K and $p = 4$ mbar, at silane dilution ratio DR = 6%. The total occurrence number for all reaction events is 1×10^9 here.

treated in the regular way. Typical KMC algorithms for models with reaction rates that span very broad timescales, in our case from nanoseconds up to seconds, demand a huge computational cost. To address the problem of the wide separation of time scales in the KMC reaction events and accelerate code execution, many other schemes have been reported in literature. Typical examples include the tau-leap method of Gillespie,[75] methods that include coarse-grained species,[76] spatially adaptive coarse grained KMC methods,[77,78] continuum mesoscopic models,[79] and multiscale KMC algorithms for epitaxial film growth.[80–84] We have validated our methodology for decoupling diffusive processes from the rest of the kinetic events by confirming that the underlying Markovian random walk process results: (a) in the same diffusivity for the diffusive species and (b) in the same film growth rate and film structural properties as the original brute force KMC algorithm for the same set of physicochemical input data (e.g., silicon hydride composition), for some initial but long enough time.

To be more specific, in our KMC method a single event among all possible reactions other than diffusion is carried out, which is then followed by a markovian diffusive random walk of the physisorbed radicals on the lattice. The number of random walk steps (denoted as n_{itype}) is different for each type of radicals (SiH_3, H, Si_2H_5) and, in addition, varies with silane DR. If l different radical types are adsorbed on the film at a certain KMC step, the total number (k) of all random walk steps to be performed at this step is given by the sum

$$k = \sum_{itype=1}^{l} n_{itype}. \tag{9}$$

In addition, since the diffusive rate is different between radicals, a variable propagation time step (Δt_{itype}) is assigned to each radical type, and the time after a successful random walk is then updated according to $t = t + \Delta t_{itype}$. The total time τ taken for diffusion in a KMC step is thus calculated as

$$\tau = \sum_{itype=1}^{l} \Delta t_{itype} n_{itype}. \tag{10}$$

At each KMC step, a reaction event (excluding diffusion) is carried out and we get prepared for starting the markovian random walk by introducing a propagator that keeps track of physisorbed radicals and their positions on the lattice. We randomly choose a physisorbed radical, make it perform a single random jump onto a neighboring site, and propagate the time accordingly. A new site in the next position is randomly selected and time is again propagated until each radical type has performed a number of n_{itype} jumps on the lattice. The diffusive time step (Δt_{itype}) of the physisorbed radicals is determined so as to reproduce the diffusivity evaluated by the corresponding brute-force KMC simulation. Like n_{itype}, Δt_{itype} is also different for different radicals (SiH_3, H, Si_2H_5) and changes with silane DR. The details are described as follows: Initially we conduct a brute-force KMC simulation and evaluate the diffusion coefficient D_s^{itype} for each radical type based on the Einstein equation for diffusion in a three-dimensional space:

$$D_s^{itype} = \frac{1}{6} \lim_{t\to\infty} \frac{\partial \left\langle r(t)^2 \right\rangle}{\partial t}, \tag{11}$$

where the mean squared displacement (msd) $\langle r(t)^2 \rangle$ is calculated as

$$\left\langle r(t)^2 \right\rangle = \frac{\sum_{i=1}^{N} [r_i(t+\tau) - r_i(\tau)]^2}{N}. \tag{12}$$

In the above equations, $r_i(t)$ is the molecule position for the ith particle at time t computed without applying periodic boundary conditions. For a three-dimensional regular lattice we can approximate the self-diffusivity by

$$D_s^{itype} = \frac{L^2}{6\Delta t_{itype}}, \tag{13}$$

where L is the (average) distance between two neighbouring sites and dt the time needed for the jump to a neighbouring site. Combining Eqs. (11) and (13) we obtain

$$\Delta t_{itype} = \frac{L^2}{\lim_{t\to\infty} \frac{\partial \left\langle r(t)^2 \right\rangle}{\partial t}}. \tag{14}$$

We note that Δt_{itype} and n_{itype} (which are system-specific) constitute the two main parameters governing the diffusive motion of physisorbed chemical species. It is thus important to know them as accurate as possible, consistent with the precomputed diffusivity value for a given radical species. The values of n_{itype} are determined by a trial-and-error procedure so as to reproduce the results for the silicon hydride (SiH, SiH_2, SiH_3, Si_2H_5) content in film and the film growth rate obtained from the corresponding brute-force KMC simulation. Typical values of the two parameters n_{itype} and Δt_{itype} employed for the two system conditions addressed here (DR = 5% and DR = 6%) are displayed in Table IV. We stress that the value of n_{itype} plays a critical role in determining the physical characteristics of the deposited films (such as film

This article is copyrighted as indicated in the article. Reuse of AIP content is subject to the terms at: http://scitation.aip.org/termsconditions. Downloaded to IP: 114.70.7.203 On: Tue, 10 Dec 2013 00:58:03

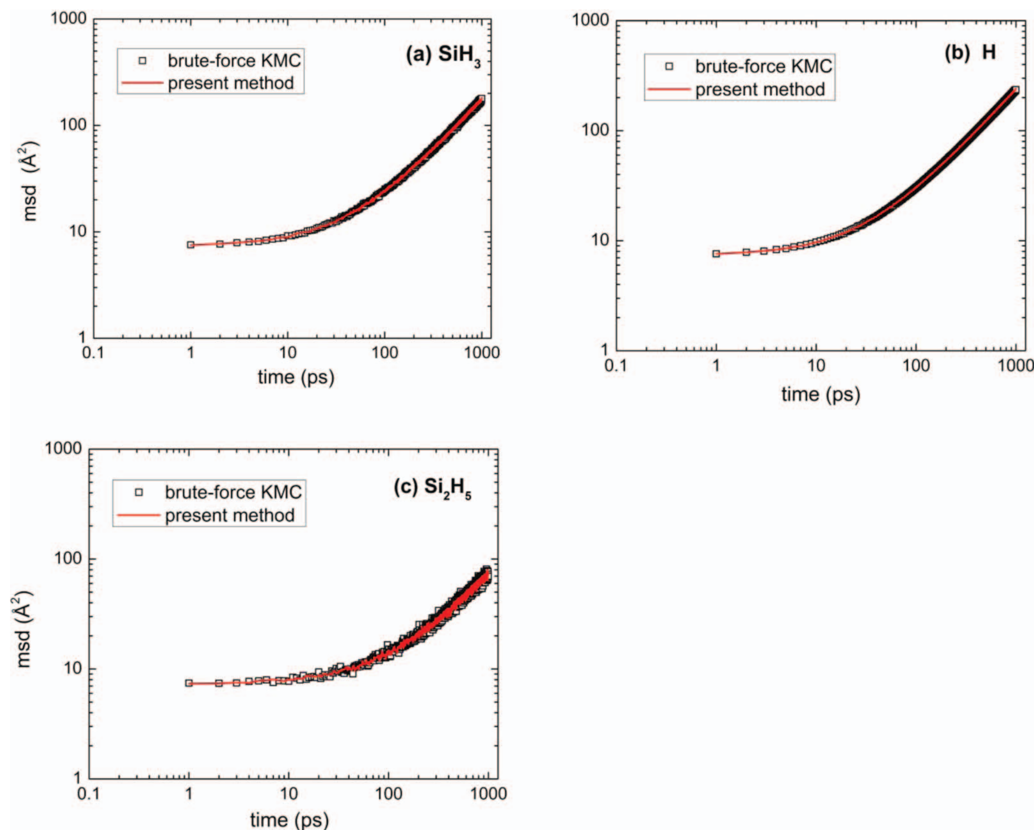

FIG. 2. Comparison for the mean squared displacement (msd) of physisorbed radicals between a brute-force execution (symbols) of the KMC algorithm and the proposed modified version treating diffusive events as Markovian processes (lines): (a) SiH_3, (b) H, and (c) Si_2H_5.

morphology and concentration of dangling bond) as it is directly associated with the mobility of physisorbed radicals and their residence time (the average time to chemisorb).

Figures 2 and 3 are indicative of the consistency between a brute-force execution of the KMC algorithm and the proposed methodology for three system properties: average mean-square displacement for radicals, silicon hydride composition, and growth rate. Excellent agreement between the two methods is documented, thereby fully validating the new, very efficient KMC methodology.

IV. RESULTS AND DISCUSSION

The substrate surface considered in this work is Si(001)-(2 × 1):H composed of approximately 2300 Si atoms. The dimension of the simulation cell is 8.5 × 9.4 nm^2. Standard periodic boundary conditions are applied in the *x*-*y* plane normal to the film growing direction. We consider different system conditions corresponding to three different values of the silane dilution ratio (DR) in the hydrogen-silane gas mixture defined as

$$DR = \frac{\Phi_{SiH_4}}{\Phi_{SiH_4} + \Phi_H}, \tag{15}$$

from 1% to 6%. Here Φ_{SiH4} and Φ_H are the silane and hydrogen flow rates, respectively. The silane flux varied from 10 to 60 SCCM (standard cubic centimeters per minutes) with the total flux of silane and hydrogen being equal to 1000 SCCM. All simulations were conducted at temperature $T = 453$ K and pressure $P = 4$ mbar. These system conditions are of practical relevance since they correspond to conditions for which reliable experimental data exist for the film growth rate, film crystallinity, hydrogen content, and surface roughness through ellipsometric, Raman Spectroscopy and AFM (Atomic Force Microscopy) measurements. The mole fractions of gas-phase species (see Table III) used in Eq. (4) were obtained using a well-tuned three-dimensional (3D) fluid simulator of silane/hydrogen discharges:[58,59] thus our KMC results can be compared with those from the 3D continuum fluid model as well as from experiment. Using the efficient KMC method developed in this work, we have been able to simulate very thick films consisting of several hundreds of monolayers at various DRs (=1%, 5%, and 6%).

A direct comparison for the rate of deposition (film growth) between the present KMC simulations and experiments is reported in Fig. 4, for a power equal to 310 mW/cm^2 and a total flow rate equal to 1 slm (standard liter per minute). Not only good qualitative but also quantitative agreement between experiment and simulations is observed demonstrating the validity of our KMC methodology and the accuracy of the selected chemical model. The systematic numerical deviations are considered to be partly due to the exclusion of gas-phase ionic species and to an underestimation of the sticking coefficients calculated from the 3D fluid model. In Fig. 5 we analyze the hydrogen content in the simulated Si films. Despite some quantitative deviations, the simulations are capable of reproducing quite well the general trends observed in the experiments for the dependence of H-content on DR.

This article is copyrighted as indicated in the article. Reuse of AIP content is subject to the terms at: http://scitation.aip.org/termsconditions. Downloaded to IP: 114.70.7.203 On: Tue, 10 Dec 2013 00:58:03

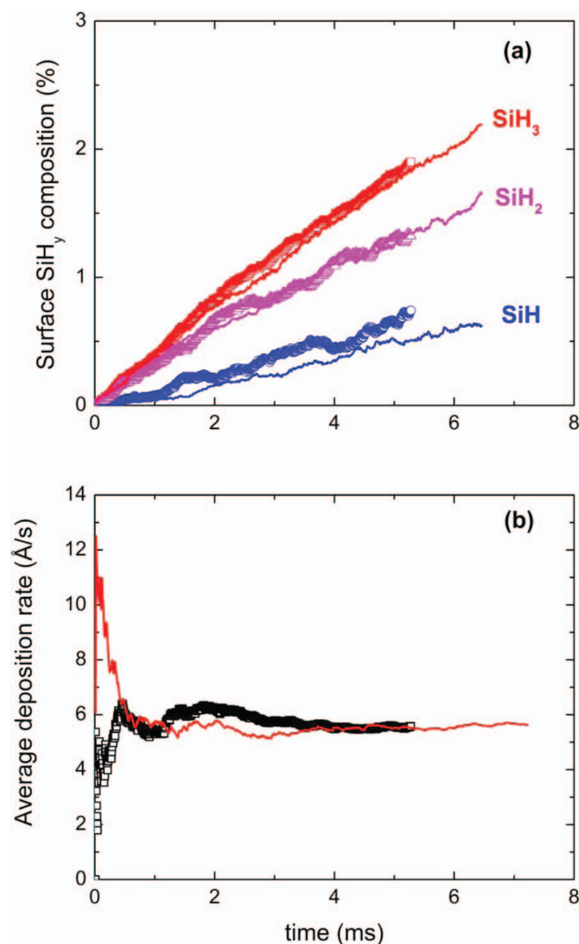

FIG. 3. Comparison of the predictions of the brute-force KMC (symbols) and of the present methodology (lines) for: (a) the silicon hydride composition in the film and (b) the deposition rate.

Simulations are seen to predict somewhat higher values of H content than what is measured experimentally, which should be attributed to the lower concentration of dangling bonds. This results in slower rates of film growth, which is consistent with the results shown in Fig. 4. The experimental values reported here have been calculated from the wagging mode of Si-H vibrations as recorded in the Raman spectra.[85,86] There was no further effort to achieve a better agreement between model and experiment as the main target was the development of the code while using the most common experimental and theoretical data one can find in the literature for sticking coefficients, activation energies, and rate constants, and no parameter was fitted in order to reproduce the experimental data. A parametric analysis of these input data is expected to improve the agreement between model and experimental findings especially for the film H-content.

TABLE III. Mole fractions of gas-phase species calculated by a well-tuned three-dimensional fluid simulator (Refs. 58 and 59) for silane/hydrogen discharges at various silane DRs (=1%–6%).

	SiH_4 DR			
Mole fraction	1%	3%	5%	6%
H ($\times 10^{-5}$)	38.2	18.3	9.60	7.72
SiH_3 ($\times 10^{-5}$)	3.33	8.66	14.3	16.5
SiH ($\times 10^{-9}$)	1.80	5.84	8.88	7.91
SiH_2 ($\times 10^{-8}$)	8.42	24.4	44.3	41.7
Si_2H_5 ($\times 10^{-5}$)	1.81	4.34	8.17	9.82

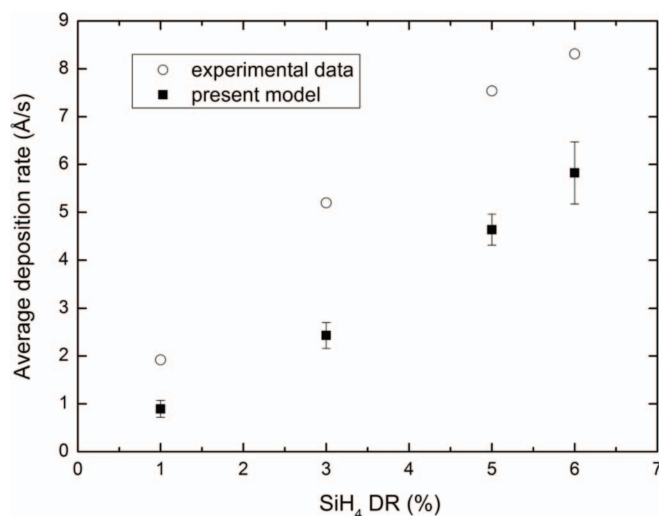

FIG. 4. Comparison between the average deposition rates obtained by the present KMC algorithm (filled squares) and from direct experimental measurements (open circles), at various silane DRs ranging from 1% to 6%.

We turn now to a detailed analysis of the individual chemical mechanisms and how they are associated with film growth, DB generation, and hydrogen elimination. We also analyze how their contributions are affected by the incoming silane flux from the gas phase. In Fig. 6, we report our KMC simulation results for the probability distribution of the reaction mechanisms that contribute to film growth at different DRs. The first five (R1, R3–R6) and the last two (R13 and R15) events constitute the chemisorption mechanisms of silicon hydride radicals via direct impingement from the gas phase upon the surface DB sites and via diffusion of physisorbed radicals onto the DB sites, respectively. From the figure it is seen that, for all DRs, the majority (∼90%) of

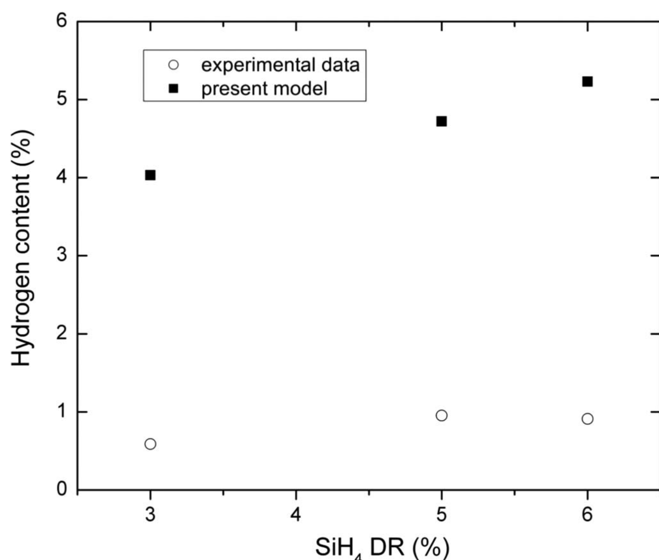

FIG. 5. Same as with Fig. 4 but for the hydrogen content.

This article is copyrighted as indicated in the article. Reuse of AIP content is subject to the terms at: http://scitation.aip.org/termsconditions. Downloaded to IP: 114.70.7.203 On: Tue, 10 Dec 2013 00:58:03

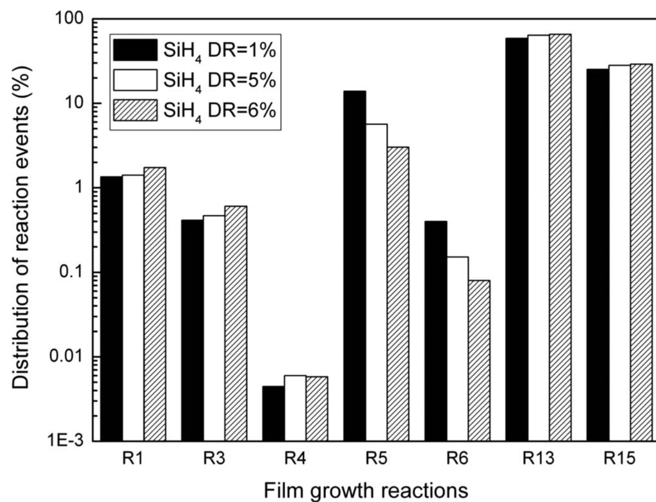

FIG. 6. Probability distribution of reaction events associated with film growth, for different silane DRs (1%, 5%, and 6%).

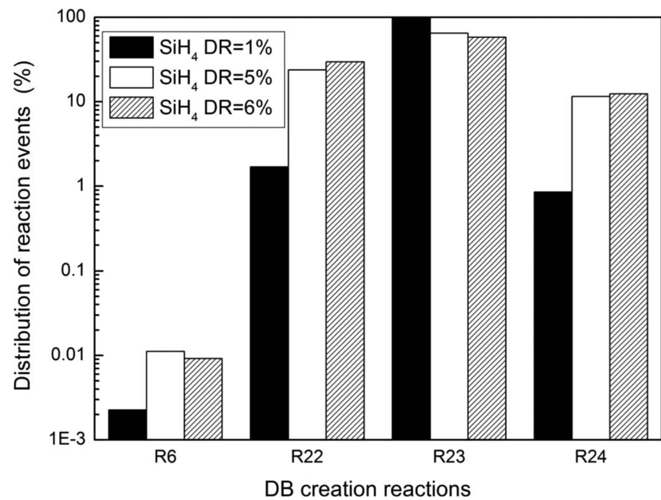

FIG. 7. Same as with Fig. 6 but for the creation of dangling bonds (DBs).

Si atoms are incorporated into the film via diffusion of physisorbed species onto DB sites, which underlines the important role of surface diffusion on film growth. This result basically corroborates the surface-diffusion model proposed by Matsuda[63–65] to explain the low temperature crystallization behavior of thin silicon films under highly diluted SiH_4 conditions (i.e., silane DR $< 10\%$) in hydrogen discharges. We also observe that the contribution of diffusive chemisorption processes to film growth increases with increasing silane DR; for example, our simulations show that it increases from 84% to 95% as the DR increases from 1% to 6%, which can be attributed to the fact that by increasing the silane DR, the formation of DB is enhanced. Over the past few years, several KMC models have appeared which neglect the diffusion of surface radicals. Our study indicates beyond any question that surface diffusion should not be neglected in PECVD simulations, because it determines the chemisorption sites of physisorbed silicon hydride radicals and thus the overall structure and quality of the film (such as surface roughness, void fractions, percentage of DB, etc.). Other important contributors to film growth from Fig. 6 are reactions R5 and R6, i.e., the direct chemisorption mechanisms of gas-phase radicals onto hydrogen-passivated sites that do not contain dangling bonds. Their total contribution is about 3% at the highest DR studied here (6%) but increases to 13% as the DR is lowered down to 1%: That the role of these reactions is diminished as the silane DR is increased reflects the relative increase of the DB concentration, which is linked with the main chemisorption mechanisms (R1, R3, R4). As we will see below, the enhanced contribution of these highly sticking and low mobile surface radicals (SiH and SiH_2) to film growth under small silane DRs is intimately connected with the columnar structures (see Fig. 11), the high porosity (see Fig. 12), and the surface roughness of the deposited films observed in the simulations, conclusions that have also been reported in the past under similar conditions.[87,88]

As dangling bonds play an important role in film growth and material properties, in Fig. 7 we report our KMC predictions for the probability distribution of reaction events that lead to DB creation at various silane DRs. Reaction R6 represents a DB formation via direct chemisorption of a highly reactive SiH radical onto a H-passivated silicon site, while R22, R23, and R24 are ER mechanisms leaving behind a DB in which a physisorbed radical [SiH_3(s), H(s), or Si_2H_5(s)] on a silicon site abstracts a hydrogen atom to form a stable gas-phase molecule [SiH_4(g), H_2(g), or Si_2H_6(g)]. According to our simulations, the overall contribution of R6 to DB creation is negligible compared to that of ER reactions. Furthermore, R23 (the DB formation mechanism accompanying evaporation of H_2(g)) appears to be the dominant one under all conditions (e.g., it contributes by more than 97% to DB formation at DR = 1%). Upon increasing the silane DR, the contribution of reactions R22 and R24 increases by more than 20 times, which is linked with the increase in the relative population of the corresponding physisorbed radicals accompanying the higher flux of silicon hydride radicals at larger DRs (see Table III). This is readily understood from the results of Fig. 8; it is indicative of the high degree of correlation between the probability distribution between

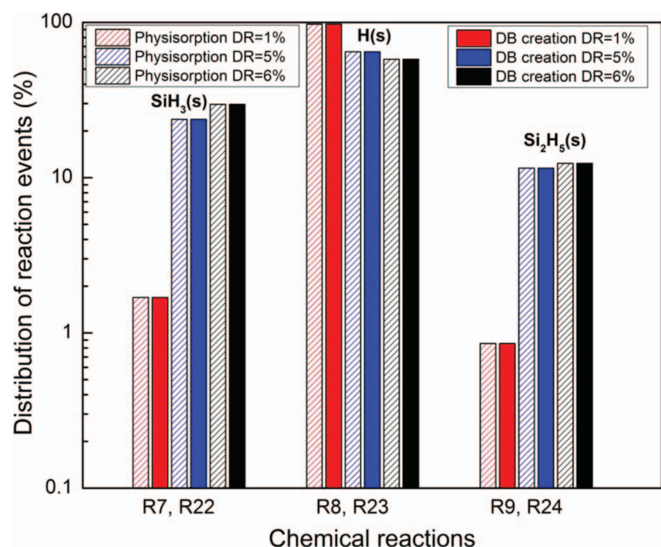

FIG. 8. One-to-one correspondence of the computed distributions for reaction events referring to physisorption and DB formation.

This article is copyrighted as indicated in the article. Reuse of AIP content is subject to the terms at: http://scitation.aip.org/termsconditions. Downloaded to IP: 114.70.7.203 On: Tue, 10 Dec 2013 00:58:03

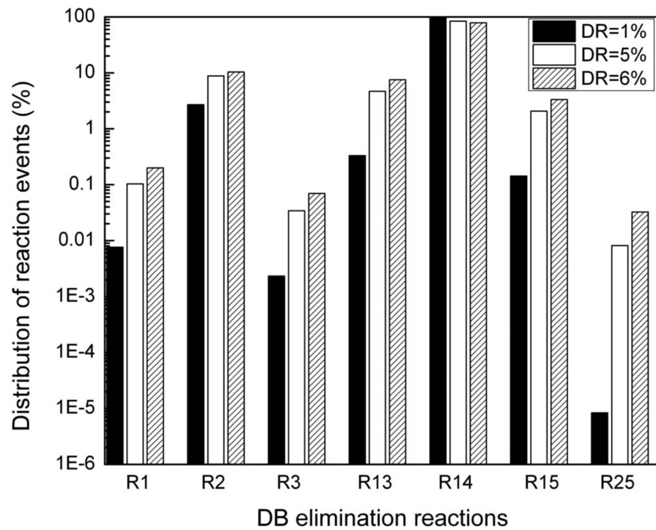

FIG. 9. Probability distribution of reaction events leading to elimination of dangling bonds, and dependence on silane DR (1%, 5%, and 6%).

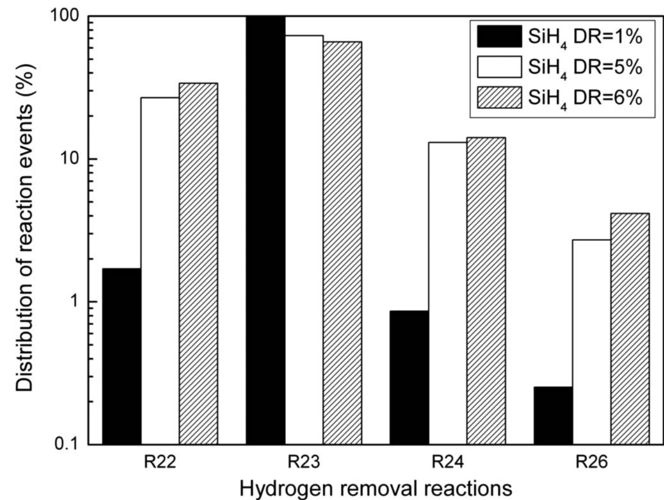

FIG. 10. Same as with Fig. 9 but for hydrogen removal.

physisorption events and the corresponding ER mechanism for each radical. Furthermore, the relative percentage of physisorption mechanisms (R7, R9) for silicon radicals increases appreciably with DR whereas that of hydrogen radicals decreases rapidly. We also notice that in the case of small DR values (1%), only a small fraction (∼3.7%) of the total physisorbed radicals leads to DB formation via reactions R22−R24; the majority of these radicals is either incorporated into the film via diffusive chemisorptions (R13−R15) or return back to the gas phase (R16−R21, R27−R29). In contrast, for high DRs, a significant increase in the fraction of the total physisorbed radicals that leads to DB formation is observed (e.g., it increases to 12.1% and then to 15.9% for DRs equal to 5% and 6%, respectively).

In understanding the intimate relationship between film growth and reaction events leading to DB creation, it is useful to further analyze the distribution of reaction mechanisms associated with DB elimination. Figure 9 illustrates that, for all conditions studied, the majority (∼93%) of DBs are removed by the hydrogen passivation reactions (R2, R14), which in turn indicates that in most cases a relatively small fraction of DBs contribute to film growth. In principle, a different mechanism that eliminates DBs is the bulkilization reaction (R25) between two neighboring DB sites, but our results show that its contribution is quite weak compared to the rest of events.

Let us look next into the mechanisms that affect the overall hydrogen content inside the grown film. As seen from Fig. 10, the major contribution comes from R22, R23, and R24. An additional but overall minor contribution comes from R26 (it amounts to ∼3% at DR = 6%), i.e., the bulkilization of two adjacent H-passivated sites evaporating hydrogen molecules. [Here we note that the contribution of physisorbed H atoms to the hydrogen content comes out from our simulations to be less than 0.1% under all system conditions; thus, for simplicity they were excluded from the analysis.] We have seen earlier in Fig. 5 that the hydrogen content in the film increases with increasing silane DR, which is consistent with experimental observations. This results mainly from the significant reduction in the flux of hydrogen atoms towards the surface (see Table III) as the DR is increased, which in turn leads to a decrease in the relative fraction of physisorbed H atoms on the surface (via R8) and thus to an appreciable reduction in the contribution of the most important reaction event (R23) to hydrogen content, as shown in Fig. 10. The fact, therefore, that our simulations overestimate the hydrogen content in the grown film (compared to the experimentally measured value) makes us believe that the value of the reaction rate for R26 used in our KMC simulations (see Table II) should have been larger.

Overall, our KMC calculations suggest that under conditions of relatively high pressure (4 mbar): (a) the main mechanism leading to film growth is the diffusive chemisorption of physisorbed SiH_3 radicals onto the DB sites (R13) and (b) the dominant mechanism for DB formation is the hydrogen abstraction by physisorbed H atom (R23). Increasing the silane mole fraction in the gas mixture reduces significantly the role of hydrogen physisorption mechanism (R8) and of the H-abstraction (R23) mechanism by physisorbed H atoms. Increasing therefore the DR results both in a higher deposition rate and a higher hydrogen content in the film, causing eventually amorphization of the deposited material; in the present work this is observed to happen for values of the DR larger than approximately 5%.

Figures 11(a) and 11(b) depict the film morphology obtained at DR = 5% and DR = 6% after the process has run for several seconds; the corresponding average thickness is 50 nm and 80 nm, respectively. It is quite remarkable to see a natural texture and several islands to emerge even under a uniform flux of gas-phase species. The deepest valley point on the surface denotes the film thickness below which all unoccupied space in the lattice is considered as voids. This thickness amounts to ∼44 nm and ∼70 nm in the two simulations (corresponding to DR = 5% and DR = 6%, respectively). The void concentration in the two films during deposition is presented in Fig. 12. At the early stages (e.g., ≤10 nm in Fig. 12) both systems exhibit the same behavior. This corresponds to the so-called incubation layer (or zone) in which any differences in the silane flux

This article is copyrighted as indicated in the article. Reuse of AIP content is subject to the terms at: http://scitation.aip.org/termsconditions. Downloaded to IP: 114.70.7.203 On: Tue, 10 Dec 2013 00:58:03

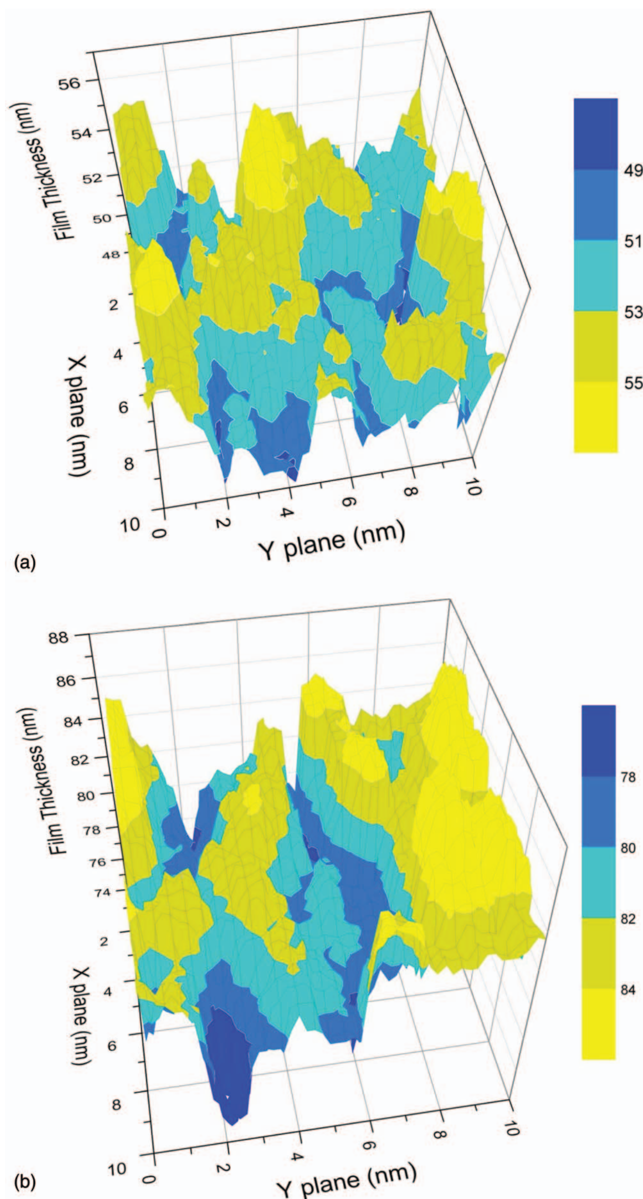

FIG. 11. Typical morphology (3D) of the free surface of one of the simulated films from the present KMC simulations at (a) DR = 5% and (b) DR = 6%. The minimum value of the height along the film surface is 44 nm and 70 nm for DR = 5% and DR = 6%, respectively. The colors of the inlet diagrams represent the length scale of the local film thickness.

(thus also in the mobility of the physisorbed species) generally do not affect void concentration.[89,90] For thick films (∼10 nm), on the other hand, the void concentration between the two systems starts to deviate from each other. The system at DR = 5% exhibits a sharp decay of the void concentration followed by a plateau (at a film thickness approximately equal to 20 nm) at around 2.5% of void fraction, whereas the DR = 6% system shows a gradual decay of its void fraction toward a plateau value of approximately 7.9% (at a film thickness equal to 60 nm). In general, a sudden increase in void concentration is typically observed in the transition regime from μc-SiH to a-Si:H growth, with the material deposited in-between characterized by inferior properties due to the presence of a larger number of voids and a larger overall hydrogen content.[90]

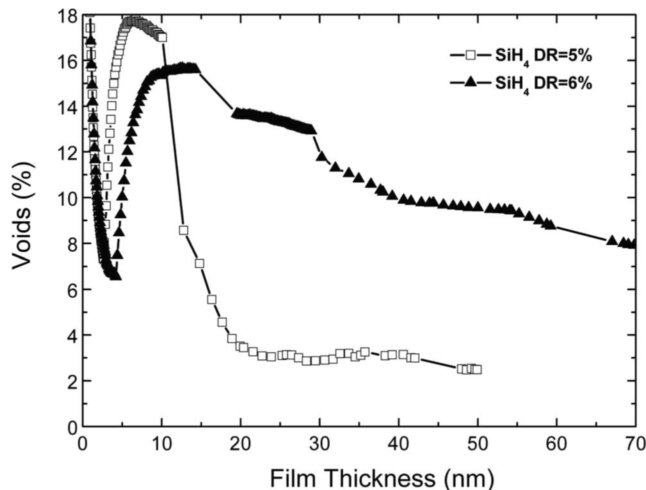

FIG. 12. Evolution of the concentration of voids in the deposited films with respect to the transient film thickness in the course of the KMC simulations at silane DR of 5% (open squares-□) and 6% (triangle-▲).

Overall, increasing the silane DR is considered to enhance film amorphization, which should be the case in our simulations with the DR = 6% system. This phenomenon can be understood in terms of the radicals' residence time in the films: as the silane DR increases, the number of DB sites increases while the residence time of physisorbed surface radicals decreases due to their enhanced participation in film growth processes via diffusive chemisorption (R13−R15). The variation of the residence time of physisorbed radicals with silane DR is featured in the present KMC simulations in the number of random walk steps (n_{itype}). As seen in Table IV, n_{itype} (and thus the residence time) increases with decreasing DR, implying that physisorbed radicals are given enough time to travel (diffuse) and penetrate deeper inside the film. For the DR = 6% system (for which n_{itype} is significantly smaller), physisorbed radicals are prone to chemisorpion on DB sites near the film surface, thus voids deeper in the film can exist for longer times during the growth process. To verify this we have calculated the probability distribution of the penetration depth (the vertical distance traveled before chemisorption) for SiH_3, H, and Si_2H_5 species at different DRs, and the results are presented in Fig. 13. Clearly, the probability for a diffusive chemisorption event to occur decreases for all radicals that have penetrated deeper in the film. More importantly, for each radical the probability for a diffusive chemisorption event at larger penetration depths is larger in the DR = 5% than in the DR = 6% system. For large penetration depths (e.g., deeper than 10 nm), in particular, the probability for a

TABLE IV. Random walk steps (n_{itype}) and random walk timestep (Δt_{itype}) for the various physisorbed radicals employed in the present KMC simulations for two different values of silane DR (5% and 6%).

	n_{itype}			Δt_{itype} (ns)		
Silane DR (%)	H	SiH_3	Si_2H_5	H	SiH_3	Si_2H_5
5	125	190	65	2.48	1.92	0.66
6	50	100	50	3.21	1.94	0.80

This article is copyrighted as indicated in the article. Reuse of AIP content is subject to the terms at: http://scitation.aip.org/termsconditions. Downloaded to IP: 114.70.7.203 On: Tue, 10 Dec 2013 00:58:03

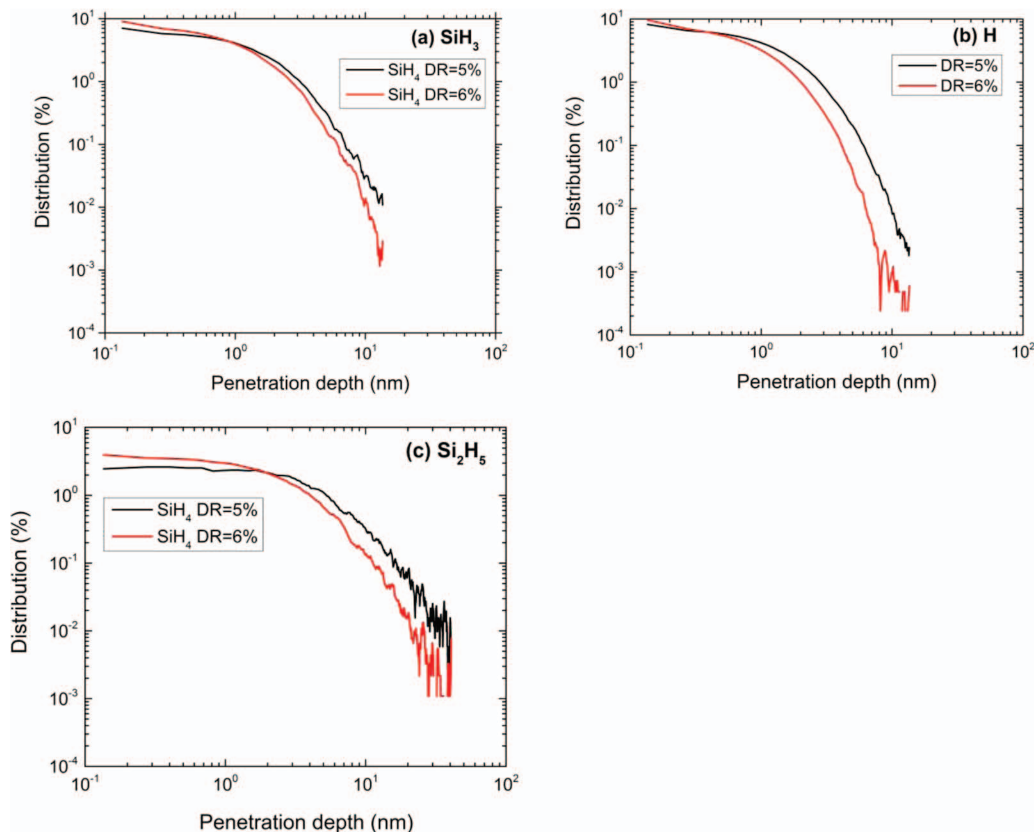

FIG. 13. Probability distribution of the penetration depth for physisorbed radicals: (a) SiH_3, (b) H, and (c) Si_2H_5, at DR = 5% and DR = 6%.

diffusive chemisorption reaction at DR = 5% is one order of magnitude larger than that at DR = 6%, which supports the above reasoning.

V. CONCLUSIONS

We have been able to model PECVD silicon film growth for long enough times (reaching film thicknesses as large as 90 nm in some cases) by a very efficient KMC method implemented along with a rich and very detailed set of chemical reactions, whose rates span a very broad range of time scales (from nanoseconds up to seconds). A key feature of our method is that it decouples the treatment of the exceedingly fast diffusive motion of all physisorbed species from that of the regular reaction events into which the considered species participate, by approximating the diffusion process via a markovian random walk. This results in a remarkable increase of computational efficiency allowing one to study sample depositions up to several hundreds of monolayers.

The new method has been extensively validated by thoroughly comparing predictions for the film growth rate, the hydrogen bonding, the silicon hydride composition in the film, and the diffusivity of all radical species against the corresponding results from a brute-force execution of the KMC algorithm; excellent agreement was documented in all cases. KMC simulation predictions with the new algorithm for the dependence of film growth rate and hydrogen content on silane fraction have been found to be in excellent qualitative and very satisfactory quantitative agreement with experimental observations. This corroborates the accuracy of the chemical model implemented, the appropriateness of the set of the important chemical species selected, and the correctness of their flux values from the gas phase towards the surface (all borrowed from an independent gas-phase simulator).

We have carried out a detailed analysis on the reaction mechanisms associated with film growth, DB formation, and hydrogen elimination, and discussed their dependence on silane fraction in the gas-phase mixture. In all cases, the most important growth mechanism turned out to be the surface diffusion of SiH_3 radicals and their subsequent chemisorption onto surface DB sties. Hydrogen abstraction by physisorbed H atoms (reaction R23) has been identified as the most significant contributor to DB creation. Upon increasing the silane fraction in the gas mixture, the population of the absorbed silicon radicals leading to hydrogen abstraction was found to increase whereas that leading to hydrogen passivation of DB sites to diminish. The net result, however, is an increase of the DB population and subsequently of the film growth rate.

We have also looked into the effect of silane fraction on the morphology (nano-scale roughness) of the deposited Si films. It was quite remarkable to see that our KMC algorithm leads to films with a natural surface texture, very similar to that observed in experimental measurements. For example, and despite the uniform flux of radicals towards the surface assumed in the simulations, the resulting films are characterized by an inhomogeneous surface roughness and voids (this is mainly the result of the diffusion process of surface

This article is copyrighted as indicated in the article. Reuse of AIP content is subject to the terms at: http://scitation.aip.org/termsconditions. Downloaded to IP: 114.70.7.203 On: Tue, 10 Dec 2013 00:58:03

radicals) resulting in a texture whose structural details resemble very much those observed in the corresponding experimental systems.

At the initial stage of film deposition, the KMC model implemented in this work is found to predict the formation of an incubation layer quite rich in voids. Beyond this layer, film growth is observed to be very sensitive to the system condition (e.g., silane DR), corresponding to the transition regime between μc-SiH and a-Si:H film growth. In our simulations, the incubation layer is observed to evolve to a dense material with a relatively small fraction of voids for the systems characterized by a dilution ratio equal to 5% (more crystalline), whereas the material grows with a large fraction of voids and high hydrogen content when the silane dilution ratio is increased to 6% (more amorphous), due to the decrease of the ad-species mobility. Future work will be directed toward the development of a multiscale simulation tool combining the present KMC method with an atomistic simulator, which will enable us to gain a deeper, direct atomistic-level insight into the important physico-chemical mechanisms governing film growth and film morphology (structure and crystallinity), as well as to get a better understanding of the relationship between conditions under which film deposition takes place and final material properties.

ACKNOWLEDGMENTS

This work is part of ongoing research work funded by the European Commission under the 7th Framework Programme (FP7-ENERGY-2009-TREN-2) titled: "Demonstration of high performance processes and equipments for thin film silicon photovoltaic modules produced with lower environmental impact and reduced cost and material use (PEPPER)." The computational work was supported by the LinkSCEEM-2 project, funded by the European Commission under the 7th Framework Programme through the Capacities Research Infrastructure, INFRA-2010-1.2.3 Virtual Research Communities, Combination of Collaborative Project and Coordination and Support Actions (CP-CSA) under Grant Agreement No. RI-261600. The authors acknowledge that the developments outlined in this paper have been achieved with the assistance of high performance computing resources provided by Cy-Tera/LinkSCEEM on NARSS, located in Egypt. The assistance of Mohammed Gaafar and Mohammed Adel from Bibliotheca Alexandria, Egypt in achieving the technical requirements is gratefully acknowledged. C.B. acknowledges financial support by UNIST (Grant Nos. 1.120023.01 and 1.110043.01).

[1]R. Reif, "Plasma enhanced chemical vapor deposition of thin films for microelectronics processing," in *Handbook of Plasma Processing Technology: Fundamentals, Etching, Deposition, and Surface Interactions*, edited by S. M. Rossnagel, J. J. Cuomo, and W. D. Westwood (Noyes Park Ridge, NJ, 1990).
[2]L. Crowley, Solid State Technol. **35**, 94 (1992).
[3]A. Shah, P. Torres, R. Tscharner, N. Wyrsch, and H. Keppner, Science **285**, 692 (1999).
[4]W. C. Sinke, MRS Bull. **18**(10), 18 (1993).
[5]A. Matsuda, Jpn. J. Appl. Phys., Part 1 **43**, 7909 (2004).
[6]D. Maroudas, Adv. Chem. Eng. **28**, 251 (2001).
[7]D. B. Graves, M. J. Kushner, J. W. Gallagher, A. Garscadden, G. S. Oehrlein, and V. A. Phelps, *Panel on Database Needs in Plasma Processing* (National Academy Press, Washington, DC, 1996).
[8]F. Paritosh, D. J. Srolovitz, C. C. Battaile, X. Li, and J. E. Butler, Acta Mater. **47**, 2269 (1999).
[9]P. Smereka, X. Q. Li, G. Russo, and D. J. Srolovitz, Acta Mater. **53**, 1191 (2005).
[10]D. D. Perovic, G. C. Weatherly, J. P. Noel, and D. C. Houghton, J. Vac. Sci. Technol. B **9**, 2034 (1991).
[11]D. D. Perovic, G. C. Weatherly, P. J. Simpson, P. J. Schultz, T. E. Jackman, G. C. Aers, J. P. Noel, and D. C. Houghton, Phys. Rev. B **43**, 14257 (1991).
[12]U. E. G. P. M. Baghbanan, Phys. Status Solidi A **203**, 1259 (2006).
[13]L. Dong and D. J. Srolovitz, J. Appl. Phys. **84**, 5261 (1998).
[14]R. W. Smith and D. J. Srolovitz, J. Appl. Phys. **79**, 1448 (1996).
[15]R. W. Smith, F. Ying, and D. J. Srolovitz, *Growth and Texture of Polycrystalline Thin Films* (Materials Research Society, Pittsburgh, PA, 1996).
[16]A. B. Bortz, M. H. Kalos, and J. L. Lebowitz, J. Comp. Phys. **17**, 10 (1975).
[17]D. T. Gillespie, J. Comp. Phys. **22**, 403 (1976).
[18]F. A. Houle and W. D. Hinsberg, Surf. Sci. **338**, 329 (1995).
[19]C. C. Battaile, D. J. Srolovitz, and J. E. Butler, J. Appl. Phys. **82**, 6293 (1997).
[20]R. W. Smith, J. Appl. Phys. **81**, 1196 (1997).
[21]U. Wetterauer, J. Knobloch, P. Hess, and F. A. Houle, J. Appl. Phys. **83**, 6096 (1998).
[22]M. Grujicic and S. G. Lai, J. Mater. Sci. **34**, 7 (1999).
[23]M. Kotrla and P. Smilauer, Phys. Rev. B **53**, 13777 (1996).
[24]H. Yan, Phys. Rev. Lett. **68**, 3048 (1992).
[25]S. Das Sarma, C. J. Lanczycki, S. V. Ghaisas, and J. M. Kim, Phys. Rev. B **49**, 10693 (1994).
[26]M. Schimschak and J. Krug, Phys. Rev. B **52**, 8550 (1995).
[27]C. J. Lanczycki, V. Jejjala, and S. Das Sarma, Phys. Rev. E **54**, 4755 (1996).
[28]P. L. Novikov, A. Le Donne, S. Cereda, Leo Miglio, S. Pizzini, S. Binetti, M. Rondanini, C. Cavallotti, D. Chrastina, T. Moiseev, H. von Kanel, G. Isella, and F. Montalenti, Appl. Phys. Lett. **94**, 051904 (2009).
[29]S. Cereda, M. Ceriotti, F. Montalenti, M. Bernasconi, and L. Miglio, Phys. Rev. B **75**, 235311 (2007).
[30]S. Cereda, F. Zipoli, M. Bernasconi, L. Miglio, and F. Montalenti, Phys. Rev. Lett. **100**, 046105 (2008).
[31]S. Cereda, Ph.D. thesis, University of Milano-Bicocca, 2007.
[32]S. Pandey, T. Singh, and D. Maroudas, J. Chem. Phys. **131**, 034503 (2009).
[33]T. Bakos, M. Valipa, E. S. Aydil, and D. Maroudas, Chem. Phys. Lett. **414**, 61 (2005).
[34]T. Bakos, M. S. Valipa, and D. Maroudas, J. Chem. Phys. **126**, 114704 (2007).
[35]M. S. Valipa, T. Bakos, E. S. Aydil, and D. Maroudas, Phys. Rev. Lett. **95**, 216102 (2005).
[36]T. Singh, M. S. Valipa, T. J. Mountziaris, and D. Maroudas, Appl. Phys. Lett. **90**, 251915 (2007).
[37]M. S. Valipa, T. Bakos, and D. Maroudas, Phys. Rev. B **74**, 205324 (2006).
[38]T. Bakos, M. S. Valipa, and D. Maroudas, J. Chem. Phys. **125**, 104702 (2006).
[39]M. S. Valipa, E. S. Aydil, and D. Maroudas, Surf. Sci. **572**, L339 (2004).
[40]J. Krug, M. Plischke, and M. Siegert, Phys. Rev. Lett. **70**, 3271 (1993).
[41]M. Siegert and M. Plischke, Phys. Rev. E **50**, 917 (1994).
[42]J. Krug, Adv. Phys. **46**, 139 (1997).
[43]P. Zhang, X. Zheng, S. Wu, and D. He, Comput. Mater. Sci. **30**, 331 (2004).
[44]G. H. Gilmer, H. Huang, T. D. de la Rubia, J. Dalla Torre, and F. Baumann, Thin Solid Films **365**, 189 (2000).
[45]P. Bruschi, A. Nannini, and F. Pieri, Phys. Rev. B **63**, 035406 (2000).
[46]H. Huang and L. G. Zhou, J. Comput.-Aided Mater. Des. **11**, 59 (2004).
[47]J. E. Rubio, M. Jaraiz, I. Martin-Bragado, J. M. Hernandez-Mangas, J. Barbolla, and G. H. Gilmer, J. Appl. Phys. **94**, 163 (2003).
[48]H. Huang and G. H. Gilmer, Comput. Mater. Sci. **23**, 190 (2002).
[49]D. J. Srolovitz, J. Vac. Sci. Technol. A **4**, 2925 (1986).
[50]D. J. Srolovitz, A. Mazor, and B. G. Bukiet, J. Vac. Sci. Technol. A **6**, 2371 (1988).
[51]S. W. Levine and P. Clancy, Modell. Simul. Mater. Sci. Eng. **8**, 751 (2000).
[52]L. Wang and P. Clancy, Surf. Sci. **473**, 25 (2001).
[53]X. Tan, Y. C. Zhou, and X. J. Zheng, Surf. Sci. **588**, 175 (2005).
[54]H. C. Huang, G. H. Gilmer, and T. D. de la Rubia, J. Appl. Phys. **84**, 3636 (1998).
[55]I. V. Sobchenko, A. M. Gusak, and K. N. Tu, "3D Monte-Carlo model of deposition and grain growth in thin films in diffusion in materials: DIMAT 2004," Pts. 1 and 2, edited by M. Danielewski, R. Filipek, R.

This article is copyrighted as indicated in the article. Reuse of AIP content is subject to the terms at: http://scitation.aip.org/termsconditions. Downloaded to IP: 114.70.7.203 On: Tue, 10 Dec 2013 00:58:03

Kozubs, W. Kucza, P. Zieba, and Z. Zurek (Trans. Tech. Publications, Stafa-Zurich, Switzerland, 2005).
[56]Y. Y. Huang, Y. C. Zhou, and Y. Pan, Physica E **41**, 1673 (2009).
[57]S. Ruan and C. Schun, J. Appl. Phys. **107**, 073512 (2010).
[58]E. Amanatides, S. Stamou, and D. Mataras, J. Appl. Phys. **90**, 5786 (2001).
[59]B. Lyka, E. Amanatides, and D. Mataras, Jpn. J. Appl. Phys. **45**, 8172 (2006).
[60]T. Ohira, O. Ukai, T. Adachi, Y. Takeuchi, and M. Murata, Phys. Rev. B **52**, 8283 (1995).
[61]T. Ohira, O. Ukai, and M. Noda, Surf. Sci. **458**, 216 (2000).
[62]V. G. Mavrantzas, "Monte Carlo simulation of chain molecules," in *The Encyclopedia of Modeling for Advanced Materials*, edited by S. Yip (Marcel Dekker, New York, NY, 2004).
[63]A. Matsuda, J. Non-Cryst. Solids **59–60**, 767 (1983).
[64]A. Matsuda, Thin Solid Films **337**, 1 (1999).
[65]A. Matsuda, J. Non-Cryst. Solids **338**, 1 (2004).
[66]S. Sriraman, S. Agarwal, E. S. Aydil, and D. Maroudas, Nature (London) **418**, 62 (2002).
[67]J. Perrin, M. Shiratani, P. Kae-Nune, H. Videlot, J. Jolly, and J. Guillon, J. Vac. Sci. Technol. A **16**, 278 (1998).
[68]A. von Keudell and J. R. Abelson, Phys. Rev. B **59**, 5791 (1999).
[69]A. Matsuda and T. Goto, Mater. Res. Soc. Symp. Proc. **164**, 3 (1990).
[70]T. Singh, M. S. Valipa, T. J. Mountziaris, and D. Maroudas, J. Chem. Phys. **127**, 194703 (2007).
[71]S. Ramalingam, D. Maroudas, and E. S. Aydil, J. Appl. Phys. **84**, 3895 (1998).
[72]S. Ramalingam, D. Maroudas, and E. S. Aydil, J. Appl. Phys. **86**, 2872 (1999).
[73]S. Ramalingam, P. Mahalingam, E. S. Aydil, and D. Maroudas, J. Appl. Phys. **86**, 5497 (1999).
[74]S. Sriraman and E. S. Aydil, J. Appl. Phys. **95**, 1792 (2004).
[75]D. T. Gillespie, J. Chem. Phys. **115**, 1716 (2001).
[76]T. O. Drews, R. D. Braatz, and R. C. Alkire, Int. J. Multiscale Comp. Eng. **2**, 313 (2004).
[77]M. A. Katsoulakis and D. G. Vlachos, J. Chem. Phys. **119**, 9412 (2003).
[78]M. A. Katsoulakis, A. J. Majda, and D. G. Vlachos, J. Comput. Phys. **186**, 250 (2003).
[79]A. Chatterjee, M. A. Snyder, and D. G. Vlachos, Chem. Eng. Sci. **59**, 5559 (2004).
[80]T. P. Schulze, P. Smereka, and E. Weinan, J. Comput. Phys. **189**, 197 (2003).
[81]C. C. Chou and M. L. Falk, J. Comput. Phys. **217**, 519 (2006).
[82]L. Mandreoli, J. Neugebauer, R. Kunert, and E. Scholl, Phys. Rev. B **68**, 155429 (2003).
[83]J. P. DeVita, L. M. Sander, and P. Smereka, Phys. Rev. B **72**, 205421 (2005).
[84]A. Chatterjee and D. G. Vlachos, J. Comput.-Aided Mater. Des. **14**, 253 (2007).
[85]U. Kroll, J. Meier, A. Shah, S. Mikhailov, and J. Weber, J. Appl. Phys. **80**(9), 4971 (1996).
[86]A. A. Langford, M. L. Fleet, and B. P. Nelson, Phys. Rev. B **45**, 13367 (1992).
[87]E. Vallat-Sauvain, U. Kroll, J. Meier, N. Wyrsch, and A. Shah, J. Non-Cryst. Solids **266**, 125 (2000).
[88]N. Wyrsch, P. Torres, M. Goerlitzer, E. Vallat, U. Kroll, A. Shah, A. Poruba, and M. Vanecek, Solid State Phenom. **67**, 89 (1999).
[89]O. Vetterl, A. Lambertz, A. Dasgupta, F. Finger, B. Rech, O. Kluth, and H. Wagner, Sol. Energy Mater. Sol. Cells **66**, 345 (2001).
[90]P. Roca i Cabarrocas, J. Non-Cryst. Solids **266**, 31 (2000).

This article is copyrighted as indicated in the article. Reuse of AIP content is subject to the terms at: http://scitation.aip.org/termsconditions. Downloaded to IP: 114.70.7.203 On: Tue, 10 Dec 2013 00:58:03